



Anisotropy of Doped Transition-Metal Magnets

R. SKOMSKI¹, V. SHARMA¹, B. BALAMURUGAN², J. E. SHIELD¹, A. KASHYAP³, D. J. SELLMYER²

¹ Department of Physics and Astronomy and Nebraska Center for Materials and Nanoscience, University of Nebraska, Lincoln, NE 68588

² LNM Institute of Information Technology, Jaipur-302031, Rajasthan, India

³ Department of Mechanical Engineering and Nebraska Center for Materials and Nanoscience, University of Nebraska, Lincoln, NE 68588

Abstract: *Calculations of the magnetocrystalline anisotropy are used to evaluate prospects for new lanthanide-free permanent magnets. Based on the requirement of transition-metal-rich phases, we investigate interstitial impurities in tetragonally distorted bcc Fe and substitutional impurities in hcp Co, and compare doped bulk materials with nanostructures, especially with elemental 3d and YCo₅ nanoparticles. Ab-initio simulations yield the dopants' net magnetization and second-order anisotropy contributions, and calculated uniaxial anisotropy constants per unit fraction of impurity atoms are 7.7 MJ/m³ (C in Fe), 3.9 MJ/m³ (N in Fe) and 11.8 MJ/m³ (Pd in Co). The examples of transition-metal and YCo₅ nanoparticles show that nanostructuring has a pronounced and difficult-to-predict effect on the anisotropy.*

Key words: *magnetic anisotropy, steel, Fe-Pd, carbides, nitrides*

Address: Ralph Skomski, E-mail: rskomski@neb.rr.com

1. Introduction

The modification of simple ferromagnetic compounds by interstitial and substitutional additives, as epitomized by martensitic steel and soft-magnetic Fe-Si, was one of the earliest research areas in magnetism [1, 2]. In fact, until the discovery of rare-earth permanent magnets around 1970, transition metal magnets had dominated progress in permanent magnetism, as exemplified by L1₀-ordered CoPt, alnico magnets, and BaFe₁₂O₁₉ [3]. Element-strategic considerations have sparked renewed interest in rare-earth-free permanent magnets, based exclusively on 3d, 4d, and 5d elements. However, to ensure a high magnetization and to limit raw-materials costs, one needs magnets rich in late 3d metals and the creation of magnetocrystalline anisotropy becomes a major concern. The problem is epitomized by the only modest magnetic anisotropy of hard-magnetic steel, but similar challenges arise in Fe- and Co-rich alloys with heavy elements such as Pd and Pt.

Surprisingly little is known about the magnetic anisotropy of steels (iron-carbon alloys). The anisotropy of hard-magnetic steel is usually explained as a strain effect [4]. Based on the magnetocrystalline anisotropy and magnetostriction of Fe-series transition metals, moderate lattice strain yields indeed magnetocrystalline anisotropies of the right order of magnitude [3]. In fact, FeCo combines a large magnetization with a large magnetostriction constant, $\lambda_{100} = 75 \cdot 10^{-6}$, and would yield, according to $\Delta K = 3\lambda_{100}\sigma/2$, a huge anisotropy if uniaxially strained [3]. Such permanent magnets have actually been proposed in the literature [5, 6], but the necessary stress σ corresponds to unphysically large *c*-axis expansion of 23%. Experimental room-temperature anisotropies atom reach about 2.1 MJ/m³, but this value does not account for the large amount of Pt (about 75 vol.%)

necessary to stabilize the structure [6]. In fact, it may be more promising to use small amounts of Pt and Pd embedded in Fe or Co.

There are various calculations on structural properties, such as interactions between interstitial atoms [7], and on magnetic order [8] and magnetic anisotropy [9, 10, 11] in stoichiometric compounds and multilayers. However, the magnetic anisotropy of doped transition metals is not very well understood, despite the fact that the basic relationship between crystal-field level splitting, spin-orbit coupling, and anisotropy has been known for almost a century [12]. One reason is that advanced first-principle calculations became available only after focus had switched to rare-earth permanent magnets. Another reason is that recent research on transition-metal alloys has largely been fueled by developments in magnetic recording, where materials requirements are different from permanent magnetism.

This paper deals with the question how the magnetic anisotropy is modified by seemingly minor structural changes, such as impurities in Fe and Co.

2. Scientific Background

2.1. Interstitial Modification

It is well-known that small amounts of carbon [1] and nitrogen [13] in α -iron occupy the octahedral interstitial sites of the bcc structure, which causes a martensitic lattice distortion. Figure 1 illustrates the location of the interstitial atoms in the middle of the faces of the bcc unit cell. The tetragonal martensitic distortion ($c > a$) is a consequence of the smallness of the octahedral interstitial site in the bcc structure. First, the hardcore radius R_i of the octahedral interstitial site is only $(2/3 - 1) R_{Fe}$

$= 0.19 \text{ \AA}$, but atoms such as C and N can be accommodated with the help of a lattice distortion. This distortion is facilitated by the flat shape of the interstitial hole. In the specific arrangement of Fig. 1, the interstitial atoms are coordinated by nearest neighbors along the c -axis, which leads to a lattice expansion in the c -direction and a contraction in the a - b -plane. Second, the elastic energy created by the local strain favors a macroscopic arrangement of the interstitial occupancy, so that the martensitic c -axis remains well-defined for rather big crystallites. This martensitic lattice distortion is responsible for both the mechanical hardness and the anisotropy (magnetic hardness) of steel.

Carbon has an atomic radius of 0.77 \AA . As one can show by treating Fig. 1 as a hard-core model, this radius corresponds to a lattice expansion of $\Delta c/c = 0.81\%$ per at.% carbon. Experimental values are of the order of $\Delta c/c = 0.59\%$ and $\Delta a/a = -0.11\%$ [1, 14, 15, 16], reflecting the low carbon concentrations encountered in practice and structural relaxations going beyond the hardcore model. Comparison of Figs. 1(b) and (c) shows that there is a big difference between lattice strain and interstitial (or substitutional) modification, even if the lattice constants are the same for both cases. Mechanical strain changes the interatomic distance by affine deformation, whereas interstitial modification actually *reduces* the interatomic distances along the c -axis. Furthermore, interstitial (and substitutional) atoms have a pronounced chemical effect, modifying the magnetic anisotropy by modifying the hybridization of the Fe and Co $3d$ orbitals.

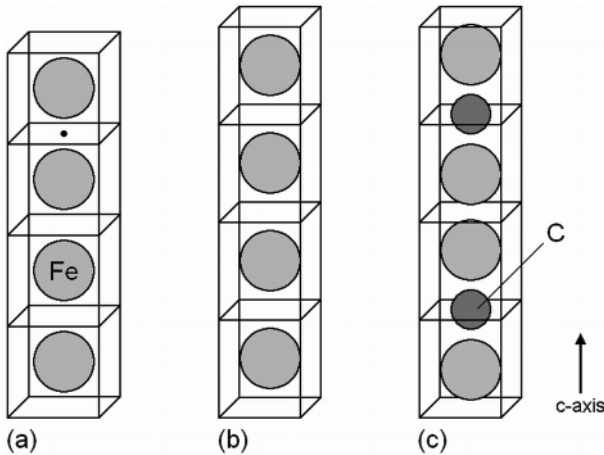


Fig. 1. Tetragonal strain in bcc iron and its relation to the octahedral interstitial site (black dots): (a) unstrained bcc Fe, (b) tetragonally strained bcc Fe with $c > a$, and (c) martensitic lattice distortion ($c > a$). In (b) and (c), the interatomic distances in the c -direction are enhanced and reduced, respectively, with far-reaching consequences for the magnetocrystalline anisotropy. For simplicity, the corner atoms of the bcc unit cells are omitted.

2.2. Origin of Anisotropy

As established long ago [12, 17], magnetocrystalline anisotropy is a combined spin-orbit and crystal-field (CF) effect. Anisotropies in both rare-earth and itinerant magnets are largely single-ion, that is, each d atom

yields an individual anisotropy contribution determined by the atom's spin-orbit interaction. In a narrow sense, the crystal-field interaction reflects the on-site energies of the magnetic and nonmagnetic atoms in the crystal. The CF contribution is sometimes regarded as the leading consideration in transition-metal oxides [12, 18, 19], but interatomic hybridization (hopping) is usually non-negligible and tends to obscure the crystal-field effect [20, 21]. In metals, the band formation due to hopping is more important than the electrostatic CF interaction [3, 17]. Advanced first-principle calculations, as used below, automatically include both hybridization and crystal-field contributions.

Compared to rare-earth anisotropies, the understanding of structure-property relationships for itinerant $3d$, $4d$, and $5d$ anisotropies is much less developed. It is possible to calculate the anisotropy numerically [17, 10], but there are no rules predicting how atomic substitutions change the anisotropy of rare-earth-free permanent magnets. This leads to complicated and generally oscillating dependence of anisotropy and orbital moment on chemical composition, atomic structure [22, 23], and, as we will discuss below, nanostructure. However, the magnitude of the second order or uniaxial anisotropy is easily estimated as λ^2/W , where W is the crystal-field or band-structure level splitting. The spin-orbit coupling constant λ is about 50 meV for Fe and Co, but about one order of magnitude bigger for heavy transition metals, such as Pd and Pt.

3. Calculations and Results

Figure 2 shows the structures considered in our first-principle calculations. The lattice constants taken for the bcc structure of Fig. 1(a) are $a = 2.755 \text{ \AA}$ and $c = 3.444 \text{ \AA}$ (Fe-C) and $a = 2.590 \text{ \AA}$ and $c = 3.288 \text{ \AA}$ (Fe-N). The calculation of the hexagonal Fe-Pd structure of Fig. 2(b) assumes the interatomic distance of elemental Co, 2.506 \AA . These lattice constants roughly correspond to available experimental data (Sect. 2.1), but no relaxation analysis has been performed at this stage.

To compute the electronic and magnetic properties of C and N in bcc and Pd in hcp Co, we have used the full-potential linear augmented plane wave (FP-LAPW) method [24]. Exchange and correlation are treated within the generalized gradient approximation (GGA) of Wu and Cohen [25]. To achieve energy eigenvalue convergence, the wave functions in the interstitial region were expanded into plane waves with a cut-off wave vector $K_{max} = 7/R_{MT}$ where R_{MT} denotes the smallest atomic sphere radius. We have taken R_{MT} values of 1.34, 1.11, 1.11 and $1.34 a_0$ for Fe, C, N and Pd, respectively. The valence wave functions inside the spheres are expanded up to $l_{max} = 10$, while the charge density was Fourier-expanded up to $G_{max} = 12$. The integrals over the Brillouin zone (BZ) are performed using 501 k -points for Fe doped with C and N. The BZ integrations were carried out using the tetrahedron method [26].

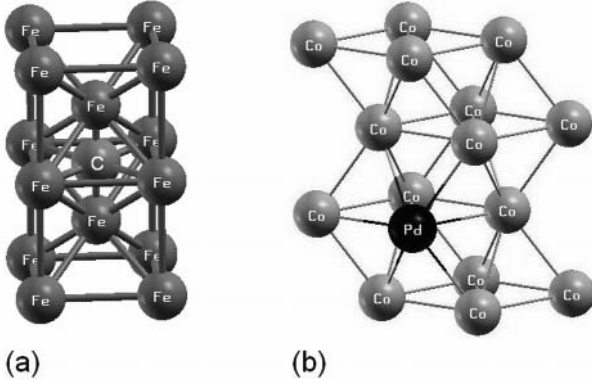


Fig. 2. Crystal structures used in the first-principle calculations: (a) carbon (or nitrogen) occupying an octahedral interstitial site in a bcc supercell and (b) substitutional Pd in hcp cobalt.

Near the Fermi level (E_F), the calculations reveal a strong coupling between the $2p$ orbitals of C and the $3d$ orbitals of nearby Fe atoms. It is instructive to use charge-density plots to visualize the hybridization between impurity and transition-metal states. Figure 3 shows the charge density for nitrogen-doped Fe. There is a substantial distortion of the charge density near the N atom, which contributes to both magnetization and anisotropy. In particular, the hybridization reduces the magnetic moments of the Fe atoms close to the impurity. In the structures of Fig. 2(a), which have the nominal composition Fe_4X , the average iron moments are $2.10 \mu_B$ ($X = C$) and $1.92 \mu_B$ ($X = N$). This relatively low value is caused by the large concentration (25%) of the interstitial atoms in Fig. 2(a). With decreasing concentration, the average moment approaches the bulk value of bcc iron ($2.26 \mu_B$).

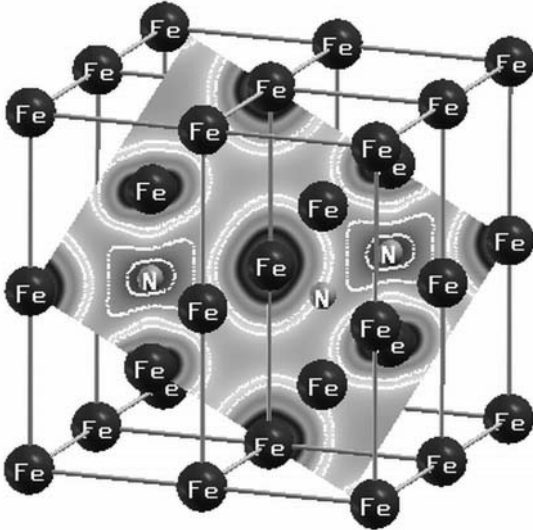


Fig. 3 Charge-density plot for atoms in a (110)-type plane of Fe-N.

Table 1 summarizes the atomic moments and anisotropies of the investigated structures. In the table, m_i , m_l , m_{II} , and m_{III} are the magnetic moments of the impurities and of their first-, second- and third-nearest Fe neighbors, respectively, and M_{av} is the volume averaged zero-temperature magnetization. E_a is the second-order

uniaxial anisotropy energy per dopant atom, obtained by comparing the magnetic energies for magnetization directions in the (001) and (100) directions, and K_1 is the volume-averaged anisotropy constant. A more detailed discussion of our results will be published elsewhere [27].

Table 1. Calculated magnetic moments and anisotropies for C and N in bcc Fe. The anisotropy values are lowest-order uniaxial anisotropy constants (K_1) and refer to unit fractions of the impurity. (Division by 100 yields the anisotropy contribution caused by 1 at. % impurities.)

	m_i	m_l	m_{II}	m_{III}	E_a	K_{th}	K_{exp}
	μ_B	μ_B	μ_B	μ_B	meV	MJ/m ³	MJ/m ³
C in Fe	-0.091	1.37	2.43	2.50	0.63 meV	7.7	5.4
N in Fe	-0.074	1.11	2.24	2.42	0.27 meV	3.9	4.4

The calculated magnetic properties are consistent with available experimental data. The magnetizations fall in the range expected for iron alloys, and the moderate reduction of the iron moment near the impurities is not surprising. Experimental anisotropy values for C and N in martensitic Fe are 0.40 meV [28, 29] and 0.32 meV [28, 30], respectively. Carbon contents are typically of the order of 0.9 wt.%, or 4 at. % ($Fe_{96}C_4$), which yields an anisotropy constant of 0.21 MJ/m³. There is some disagreement between theory and experiment, partially because experiments are limited to small impurity concentrations. An anisotropy value for $Fe_{16}N_2$ thin films is 1.6 MJ/m³ [31], although nitrogen cannot be considered as a random interstitial atom in these tetragonal compounds [13]. The anisotropy of orthorhombic Co_3Pt is of the order of 2.0 MJ/m³ [32], whereas $Co_{92}Pt_8$ has a K_1 of 0.6 MJ/m³, or 7.5 MJ/m³ per unit fraction of Pt [33].

The supercell of Fig. 2(b) corresponds to the nominal composition $Co_{15}Pd$. Our calculations yield a Pd moment of $0.36 \mu_B$ and an anisotropy energy of 1.55 meV per supercell (or Pd atom), which translates into a net anisotropy constant of 1.4 MJ/m³. The interpretation of the Pd anisotropy requires some care, because the cobalt host has a hexagonal crystal structure and a nonzero uniaxial anisotropy, about 0.7 MJ/m³ at zero temperature [34]. (The above-considered bcc-iron host has some cubic but no uniaxial anisotropy.) Subtracting the uniaxial bulk anisotropy of the 15 Co atoms in each supercell yields a Pd anisotropy of 11.8 MJ/m³ per unit fraction. In other words, about 47% of the total anisotropy of $Co_{15}Pd$ come from the Co and 53% from the Pd. This indicates that small additions of Pd yield substantial anisotropy enhancements.

4. Anisotropy of Magnetic Nanostructures

What are the prospects for creating a new lanthanide-free permanent-magnet material? Past research has explored virtually all binary and many ternary and quaternary phase diagrams, and the likelihood of an overlooked intermetallic phase is small [35]. There is, of course, a

possibility that dopants may stabilize an otherwise unstable or metastable phase, but this and other 'chemical' approaches have a rather remote chance of success. A well-known approach to improve permanent magnets is to use nanostructures based on available bulk materials, such as $\text{Nd}_2\text{Fe}_{14}\text{B}$ and $\alpha\text{-Fe}$ [35, 36, 37]. However, nanostructuring can also be used to modify the anisotropy and to create magnets with new or improved properties. Furthermore, technology has advanced since the 1960s, and recent developments in experimental nanomagnetism have opened the gate for the design of new materials. This may make it possible to stabilize structures that are unstable in the bulk form.

An intriguing question is the dependence of the anisotropy on the nanostructure. For a given material, the surface anisotropy depends on the indexing of the surface planes [38] and therefore on the faceting of the structure or particle. In addition, the well-known example of alloys of Fe, Co, and Ni [1] shows that the anisotropy is rarely a linear function of the atomic concentrations. The situation is further complicated if one simultaneously considers structure and stoichiometry. Figure 4 shows the results of a phenomenological but non-perturbative $3d$ -only tight-binding calculation for a 13-atom hcp cluster [22]. The model simulation yields strong oscillations of the anisotropy as a function of the number n of d electrons per atom, which can be tuned by alloying, similar to the control of the magnetization on the Slater-Pauling curve. (Approximate d -counts are $n = 7$ for Fe, $n = 8$ for Co, and $n = 9$ for Ni). The structural aspect comes into play by comparing hcp and fcc clusters. The corresponding 13-atom fcc cluster, which differs from Fig. 4(a) by the rotation of the top (or bottom) triangle by 60° , has a uniaxial anisotropy of exactly zero.

Since the present method lacks selfconsistency, it cannot predict accurate peak heights and positions. However, the main feature of Fig. 4, namely the occurrence of a large number of peaks and zeros, is unaffected by the present approximation. The surprising feature is not the well-known existence of peaks and zeros, but the large number of the peaks, even for relatively simple structures. This is different from Pd and Pt in $3d$ hosts, which shows a pronounced, but probably not universal, trend towards positive anisotropy constants. Note, however,

that Pd and Pt are chemically and electronically very similar congeners with the same d count.

The past few decades have seen a rapid development in nanofabrication techniques. For example, much progress has been made in the use of cluster deposition [39] to fabricate small-scale nanoparticles with well-defined atomic structures. Figure 5 shows cluster-deposited YCo_5 nanoparticles. In spite of the small particle size, about 5 nm, the YCo_5 structure is well-developed. Coercivity and loop squareness can both be tuned by modifying the deposition conditions. Preliminary experiments yield coercivities of about 1.0 T [10 kOe] at low temperatures and 0.6 T at room temperature, with a remanence ratio $M_r/M_s \approx 0.75$ [40].

5. Discussion and Conclusions

An atomic model frequently used to discuss itinerant anisotropies is the Néel model [41]. However, the Néel model assumes a pair interaction between two magnetic atoms and is unable to describe the effect of non-magnetic atoms, which affect the anisotropy by altering crystal field, level occupancy and interatomic hopping. In $L1_0$ type magnets, such as CoPt and FePd, the Néel model is also unable to distinguish between two important anisotropy contributions, namely the large $4d/5d$ anisotropy caused by $3d$ neighbors and the smaller $3d$ anisotropy created by the $4d/5d$ neighborhood [22]. Furthermore, the example of Fig. 5 shows that more distant neighbors are also important. For both the hcp cluster with ideal c/a ratio and the corresponding fcc cluster, the Néel model yields zero uniaxial anisotropy, in contrast to the finite tight-binding anisotropy of the hcp cluster. Physically, the hybridization between the d -electrons in the 13-atom clusters depends on the relative orientation of the top and bottom triangles. Alternatively, the peaks in Fig. 5 mean that small energy differences must be resolved properly, which requires the consideration of many neighbors.

In conclusion, our calculations show that relatively small impurity concentrations yield substantial anisotropy contributions. In the case of C and N in iron, the main effect is chemical and consists in a modification of the hybridization of the Fe $3d$ orbitals, but strain effects are

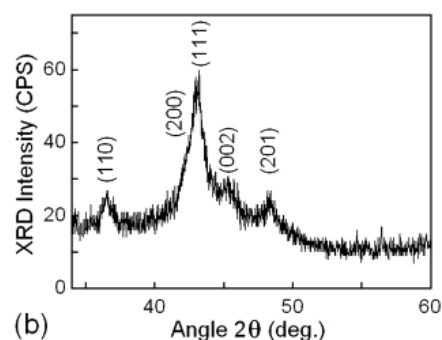
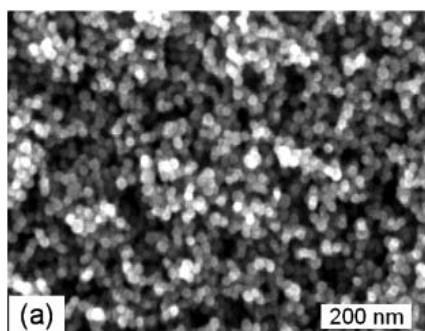


Fig. 4. Anisotropy of a hexagonal 13-atom cluster (after Ref. 22): (a) structure and (b) anisotropy as a function of the number of d electrons per atoms (d -count). For the present structure, 10 meV roughly correspond to $K_1 = 10 \text{ MJ/m}^3$.

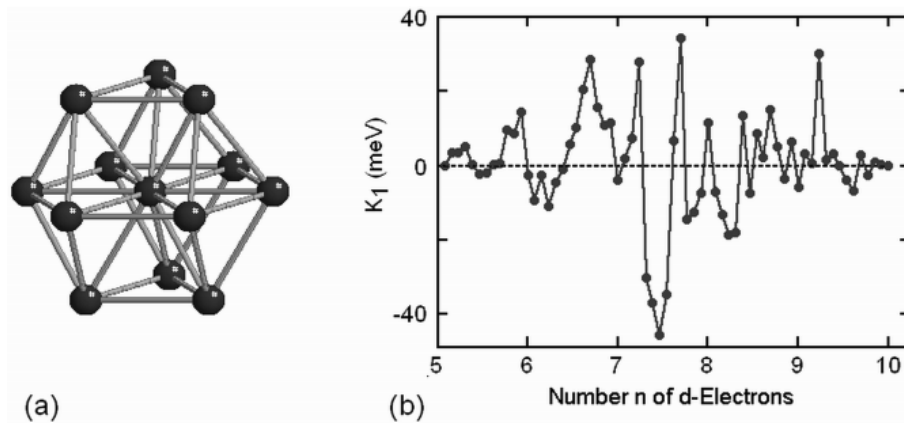


Fig. 5. YCo_5 powder produced by cluster deposition: (a) SEM picture and (b) XRD pattern. The particle size is about 6 nm.

also important. By contrast, the direct anisotropy contribution of the C and N is virtually zero, due to the small magnetization and spin-orbit coupling of the $2p$ atoms. Substitutional Pd yield a huge anisotropy contribution, caused by their large spin-orbit coupling. Doping with low concentrations of heavy transition metals in late 3d hosts is therefore one of the few alternatives to rare-earth permanent magnets, although much theoretical and experimental work remains to be done in this direction. Nanostructuring is a further option, with challenges and opportunities for future research.

Acknowledgement

The authors are thankful to P. Blaha and K. Schwarz for providing the WIEN2k code. This research is supported by DOE (D.J.S.), BREM and NSF MRSEC (R.S., J.E.S.), ARO (R.Zh.), ARPA-E (R.S., J.E.S.), NCMN, and by DST (India-EU collaborative project DYNAMAG and Nano Mission, A.K. and V.S.).

References

- [1] R. M. Bozorth, *Ferromagnetism*, van Nostrand, Princeton, New Jersey, 1951.
- [2] M. Kersten, „Zur Theorie der ferromagnetischen Hysterese und der Anfangspermeabilität“, *Z. Phys.* **44** (1943) 63-77.
- [3] R. Skomski and J. M. D. Coey, *Permanent Magnetism*, Institute of Physics, Bristol 1999.
- [4] S. Chikazumi, *Physics of Magnetism*, Wiley, New York 1964.
- [5] T. Burkert, L. Nordström, O. Eriksson, and O. Heinonen, “Giant Magnetic Anisotropy in Tetragonal FeCo Alloys”, *Phys. Rev. Lett.* **93** (2004) 027203-1-4.
- [6] G. Andersson, T. Burkert, P. Warnicke, M. Björck, B. Sanyal, C. Chacon, C. Zlotea, L. Nordström, P. Nordblad, and O. Eriksson, “Perpendicular Magnetocrystalline Anisotropy in Tetragonally Distorted Fe-Co Alloys”, *Phys. Rev. Lett.* **96** (2006) 037205.
- [7] C. Domain, C. S. Becquart, and J. Foct, “Ab initio study of foreign interstitial atom (C, N) interactions with intrinsic point defects in α -Fe”, *Phys. Rev. B* **69** (2004) 144112-1-16.
- [8] A. Kashyap, R. Skomski, A. K. Solanki, Y. F. Xu, and D. J. Sellmyer, “Magnetism of $L1_0$ Compounds with the Composition MT ($M = Rh, Pd, Pt, Ir$ and $T = Mn, Fe, Co, Ni$)”, *J. Appl. Phys.* **95** (2004) 7480-7482.
- [9] M. E. McHenry, B. Ramalingum, S. Willoughby, J. MacLaren, and S. G. Sankar, “First Principles Calculations of the Electronic Structure of $Fe_{1-x}Co_xPt$ ”, *IEEE Trans. Magn.* **37** (2001) 1277-1279.
- [10] S. Willoughby, J. MacLaren, T. Ohkubo, S. Jeong, M. E. McHenry, D.E Laughlin, S.-J. Choi and S.-J. Kwon, “Electronic, Magnetic and Structural Properties of $L1_0 FePt_xPd_{1-x}$ Alloys”, *J. Appl. Phys.* **91** (2002) 8822-8824.
- [11] S. D. Willoughby, R. A. Stern, R. Duplessis, J. M. MacLaren, M. E. McHenry and D. E. Laughlin, “Electronic structure calculations of hexagonal and cubic phases of Co_3Pt ”, *J. Appl. Phys.* **93** (2003) 7145-7147.
- [12] F. Bloch and G. Gentile, „Zur Anisotropie der Magnetisierung ferromagnetischer Einkristalle“, *Z. Phys.* **70** (1931) 395-408.
- [13] K. H. Jack, “The Occurrence and the Crystal Structure of α -Iron Nitride; a New Type of Interstitial Alloy Formed during the Tempering of Nitrogen-Martensite”, *Proc. R. Soc. A* **208** (1951) 216-224.
- [14] Y.-M. Liu U. Zh.-R. He, “Substructure and Crystal Morphology of Martensite in Medium Carbon Iron Alloys”, *Acta Metallurgica Sinica (English Edition) A* **2** (1989) 364-367.
- [15] G. K. Williamson and R. E. Smallman, “X-ray evidence for the interstitial position of carbon in α -iron”, *Acta Cryst.* **6** (1953) 361-362.
- [16] C. S. Becquart, J. M. Raulot, G. Bencteux, C. Domain, M. Perez, S. Garruchet, H. Nguyen, “Atomistic modeling of an Fe system with a small concentration of C”, *Computational Materials Science* **40** (2007) 119-129.
- [17] H. Brooks, “Ferromagnetic Anisotropy and the Itinerant Electron Model”, *Phys. Rev.* **58** (1940) 909-918.
- [18] N. Fuchikami, “Magnetic Anisotropy of Magnetoplumbite $BaFe_{12}O_{19}$ ”, *J. Phys. Soc. Japan* **20** (1965) 760-769.
- [19] H. Bethe, “Termaufspaltung in Kristallen”, *Ann. Physik [5]* **3** (1929) 133-208.
- [20] L. F. Mattheiss, “Electronic Structure of the 3d Transition-Metal Monoxides: I. Energy Band Results”,



- Phys. Rev. B **5** (1972) 290-306; "II. Interpretation", *ibidem* 306-315.
- [21] W. L. Roth, "Magnetic Structures of MnO, FeO, CoO, and NiO", Phys. Rev. **110** (1958) 1333-1341.
- [22] R. Skomski, A. Kashyap, A. Solanki, A. Enders, and D. J. Sellmyer, "Magnetic Anisotropies in Itinerant Magnets", J. Appl. Phys. **107** (2010) in press.
- [23] T. Andersen and W. Hübner, "Substrate effects on surface magnetism of Fe/W(110) from first principles", Phys. Rev. B **74** (2006) 184415-1-8.
- [24] P. Blaha, K. Schwarz, G. K. H. Madsen, D. Kvasnicka, and J. Luitz, "WIEN2K, An Augmented Plane Wave + Local Orbitals Program for Calculating Crystal Properties", Ed. K. Schwarz, Technische Universität Wien, Vienna 2008.
- [25] Zh.-G. Wu and R. E. Cohen, "More accurate generalized gradient approximation for solids", Phys. Rev. B **73** (2006) 235116-1-6.
- [26] P. E. Blöchl, O. Jepsen, and O. K. Andersen, "Improved tetrahedron method for Brillouin-zone integrations", Phys. Rev. B **49** (1994) 16223-16233.
- [27] V. Sharma *et al.*, in preparation (2010).
- [28] G. de Vries, D. W. van Geest, R. Gersdorf, and G. W. Rathenau, "Determination of the magnetic anisotropy energy, caused by interstitial carbon or nitrogen in iron", Physica **25** (1959) 1131-1138.
- [29] E. Kisdi-Koszo, G. Konczos, K. Lazar, G. Neuprandt, "Influence of interstitial impurities on the magnetic properties of pure iron", IEEE Trans. Magn. **10** (2) (1974) 175-176.
- [30] Y. Tahara and T. Sugeno, "Magnetic Anisotropy Energy Caused by Nitrogen in α -Iron", Jpn. J. Appl. Phys. **12** (1973) 1550-1552.
- [31] H. Takahashi, M. Igarashi, A. Kaneko, H. Miyajima, and Y. Sugita, "Perpendicular Uniaxial Magnetic Anisotropy of Fe₁₆N₂(001) Single Crystal Films Grown by Molecular Beam Epitaxy", IEEE Trans. Magn. **35** (5) (1999) 2982-2984.
- [32] J. M. MacLaren, R. R. Duplessis, R. A. Stern, and S. Willoughby, "First principles calculations of FePt, CoPt, Co₃Pt, and Fe₃Pt alloys", IEEE Trans. Magn. **41** (12) (2005) 4374 - 4379.
- [33] H. Yuan and D. E. Laughlin, "Effects of substrate bias on magnetocrystalline anisotropy Ku of CoPt thin films with increasing Pt content", J. Appl. Phys. **105** (2009) 07A712-1-3.
- [34] R. Skomski and D. J. Sellmyer, "Intrinsic and Extrinsic Properties of Magnetic Nanostructures," in Handbook of Advanced Magnetic Materials, eds. Y. Liu, D. Shindo, D. J. Sellmyer, Springer, Berlin 2006, pp. 1-57.
- [35] R. Skomski and J. M. D. Coey, "Giant Energy Product in Nanostructured Two-Phase Magnets", Phys. Rev. B **48** (1993) 15812-15816.
- [36] R. Coehoorn, D.B. de Mooij, and C. de Waard, "Melt-spun permanent magnet materials containing Fe₃B as the main phase", J. Magn. Magn. Mater. **80** (1989) 101-104.
- [37] E. F. Kneller, "The exchange-spring magnet: A new material principle for permanent magnets", IEEE Trans. Magn. **27** (1991) 3588-3599.
- [38] R. Skomski, "Nanomagnetics", J. Phys.: Condens. Matter **15** (2003) R841-896.
- [39] Y. F. Xu, M. L. Yan, and D. J. Sellmyer, "Cluster-Assembled Nanocomposites", in: *Advanced Magnetic Nanostructures*, Eds.: D. J. Sellmyer and R. Skomski, Springer, Berlin 2006, ch. 8, p. 207-238.
- [40] B. Balamurugan *et al.*, "Cluster-Deposited YCo₅ Magnets", in preparation (2010).
- [41] L. Néel, "Anisotropie Magnétique Superficielle et Structures d'Orientation", J. Phys. Radium **15** (1954) 225-239.